Energy-band alignment of II-VI/Zn3P2 heterojunctions from x-ray photoemission spectroscopy

Jeffrey P. Bosco, David O. Scanlon, Graeme W. Watson, Nathan S. Lewis, and Harry A. Atwater

Energy-band alignment of II-VI/Zn_3P_2 heterojunctions from x-ray photoemission spectroscopy

Jeffrey P. Bosco,[1,a)] David O. Scanlon,[2] Graeme W. Watson,[3] Nathan S. Lewis,[1] and Harry A. Atwater[1]

[1]*Watson Laboratory and Noyes Laboratory, Beckman Institute and Kavli Nanoscience Institute, California Institute of Technology, 1200E. California Blvd., Pasadena, California 91125, USA*
[2]*University College London, Kathleen Lonsdale Materials Chemistry, Department of Chemistry, 20 Gordon Street, London, WC1H 0AJ, United Kingdom*
[3]*School of Chemistry and CRANN, Trinity College Dublin, College Green, Dublin 2, Ireland*

The energy-band alignments for zb-ZnSe(001)/α-Zn_3P_2(001), w-CdS(0001)/α-Zn_3P_2(001), and w-ZnO(0001)/α-Zn_3P_2(001) heterojunctions have been determined using high-resolution x-ray photoelectron spectroscopy via the Kraut method. *Ab initio* hybrid density functional theory calculations of the valence-band density of states were used to determine the energy differences between the core level and valence-band maximum for each of the bulk materials. The ZnSe/Zn_3P_2 heterojunction had a small conduction-band offset, ΔE_C, of -0.03 ± 0.11 eV, demonstrating a nearly ideal energy-band alignment for use in thin-film photovoltaic devices. The CdS/Zn_3P_2 heterojunction was also type-II but had a larger conduction-band offset of $\Delta E_C = -0.76 \pm 0.10$ eV. A type-III alignment was observed for the ZnO/Zn_3P_2 heterojunction, with $\Delta E_C = -1.61 \pm 0.16$ eV indicating the formation of a tunnel junction at the oxide–phosphide interface. The data also provide insight into the role of the II-VI/Zn_3P_2 band alignment in the reported performance of Zn_3P_2 heterojunction solar cells. © 2013 AIP Publishing LLC. [http://dx.doi.org/10.1063/1.4807646]

I. INTRODUCTION

Zinc phosphide (α-Zn_3P_2) is a group II-V compound semiconductor with a 1.5 eV direct band gap as well as a high visible-light absorption coefficient near the band edge ($>1 \times 10^4$ cm^{-1}).[1,2] The acceptor concentration in Zn_3P_2 can be controlled from 10^{13} to 10^{18} cm^{-3} using extrinsic dopants,[3] and spectral response measurements have indicated that polycrystalline Zn_3P_2 can have minority-carrier diffusion lengths of $>5 \mu m$.[4] Zn_3P_2 is composed of earth-abundant and inexpensive elements and the compound sublimes congruently,[5] allowing for scalable, thin-film deposition via techniques such as closed-space sublimation (CSS) and physical vapor transport (PVT). In fact, a recent abundance and cost analysis has indicated that the extraction cost of Zn_3P_2 could potentially be lower than that of Si.[6] These properties thus make Zn_3P_2 an excellent candidate for use as an earth-abundant, thin-film photovoltaic (PV) material.

The fabrication of Zn_3P_2 homojunctions has been complicated by difficulties in creating low-resistivity, n-type material due to the formation of self-compensating, p-type intrinsic defects in the Zn_3P_2 crystal lattice.[7,8] Hence, the majority of PV device investigations with Zn_3P_2 has focused on Schottky barrier or heterojunction solar cells, with Table I listing the champion cell properties for devices that have incorporated Zn_3P_2 as a solar absorber. Mg Schottky structures have demonstrated the highest solar energy-conversion efficiencies, with values of ~6% for devices fabricated on PVT-grown Zn_3P_2 wafers and values of 4.3% for Zn_3P_2 thin films deposited by CSS.[4,9] However, these devices were reported to have a high concentration of interface trap states, therefore, limiting the open-circuit voltage (V_{OC}) to <500 mV due to Fermi-level pinning.[10] Optical absorption and reflection losses at the metal–semiconductor contact also place an upper limit on the attainable short-circuit current densities (J_{SC}) in photovoltaics based on a Schottky barrier structure. The combined current density and voltage restrictions of the Mg/Zn_3P_2 device thus present challenges to obtaining further improvements in the PV device efficiency of such systems.

Zn_3P_2 heterojunction solar cells have also been fabricated by use of common n-type emitters such as ZnO, Sn-doped In_2O_3 (ITO), CdS, ZnSe, and ZnS.[11–15] The solar energy-conversion efficiencies of these devices to date are less than ~2%. Nevertheless, in some cases, the V_{OC} and J_{SC} values surpass those of Mg/Zn_3P_2 Schottky barriers, suggesting that efficiency enhancements are possible through the use of a heterojunction solar cell design. Notably, the barrier heights measured for the heterojunctions are not in good agreement with those predicted from Anderson band alignment theory based on the electron affinities of the materials used to form the junction.[16] This disagreement is not unexpected because the actual band offsets often deviate from the ideal values.[17]

To understand the fundamental limitations on the attainable barrier heights of Zn_3P_2 heterojunction solar cells, we describe herein band alignment measurements on heterovalent interfaces composed of n-type II-VI semiconductors grown on the Zn_3P_2(001) surface. We have specifically investigated ZnSe, CdS, and ZnO emitters because these materials are commonly employed in photovoltaic devices

a)Author to whom correspondence should be addressed. Electronic mail: jbosco@caltech.edu

TABLE I. Device properties of champion Schottky and heterojunction solar cells that utilized a Zn_3P_2 photovoltaic absorber.

Junct. partner	[a]Partner E_g (eV)	[b]Partner χ (eV)	Absorber fab.	Area (cm^2)	η (%)	V_{OC} (mV)	[c]V_D (mV)	J_{SC} (mA cm^{-2})	ff
[4]Mg	…	3.6	PVT	0.7	5.96	492	800	14.93	0.71
[9]Mg	…	3.6	CSS	1.0	4.3	430	1320	16.8	0.53
[11]ITO	3.80	…	PVT	0.06	2.1	280	…	18.4	0.4
[12]ZnO	3.40	4.57	PVT	0.022	1.97	260	780	11	0.59
[13]CdS	2.42	4.79	PVT	0.09	1.2	300	640	11.1	0.35
[14]ZnSe	2.70	4.09	CSS	0.1	0.81	810	1480	1.55	0.5
[15]ZnS	3.68	3.9	MBE	0.35	0.01	780	…	0.05	0.35

[a]Junction partner band gap, E_g.[50,51]
[b]Junction partner work function or electron affinity, χ.[52,53]
[c]Diffusion voltage, V_D, was determined by temperature-dependent I-V measurements under 1-Sun illumination.

and have already been used in conjunction with Zn_3P_2-based photovoltaics. Using high-resolution x-ray photoelectron spectroscopy (XPS), the valence-band discontinuities (ΔE_V) between the II-VI materials of interest and Zn_3P_2 have been determined using the method of Kraut *et al.*[18] Specifically,

$$\Delta E_V = (E_{CL}^{\text{II-VI}} - E_{VBM}^{\text{II-VI}}) - (E_{CL}^{Zn_3P_2} - E_{VBM}^{Zn_3P_2}) - \Delta E_{CL,i}, \quad (1)$$

where the first two components of Eq. (1) represent the core-level (CL) to valence-band maximum (VBM) energy differences measured on thick films ($\sim$200 nm) of the II-VI compound and Zn_3P_2, respectively, and $\Delta E_{CL,i}$ represents the energy difference between the II-VI and Zn_3P_2 core levels measured on an ultrathin II-VI/Zn_3P_2 heterojunction interface. From the value of ΔE_V, the corresponding value of the conduction-band discontinuity (ΔE_C) can then be calculated from the reported values for the band gaps of the materials, according to

$$\Delta E_C = E_g^{\text{II-VI}} - E_g^{Zn_3P_2} + \Delta E_V. \quad (2)$$

This method has been used previously to determine the band discontinuities of epitaxial zb-ZnS(001)/α-Zn_3P_2(001) heterojunctions.[15]

II. EXPERIMENTAL METHODS

The II-VI/Zn_3P_2 heterostructures were fabricated on Zn_3P_2 epilayers that had been grown by compound-source molecular-beam epitaxy (MBE). The growth of Zn_3P_2 from a compound sublimation source has been studied in detail previously.[19] The Zn_3P_2 compound-source material was synthesized from elemental Zn and P (99.9999%, Alfa Aesar).[20,21] Zn-doped GaAs(001) substrates were used as an epitaxial template. The GaAs native oxide was removed by exposure to a RF-generated atomic hydrogen flux at 450 °C. The films were grown at 200 °C using a Zn_3P_2 beam equivalent pressure (BEP) of $\sim$1.5 × 10^{-6} Torr. Under these conditions, stoichiometric Zn_3P_2 films have been reported to grow epitaxially with excellent crystallinity along the (001) direction.[19]

Zinc-blende ZnSe and wurtzite CdS films were also grown by compound-source MBE in the same vacuum chamber. ZnSe films have been reported to grow using congruent

sublimation from a compound source with similar crystalline and optoelectronic quality to films grown with separate elemental sources.[22,23] Vacuum evaporation of CdS from a compound source is a standard deposition technique for PV applications.[24,25] In this work, ZnSe was grown at 200 °C at a BEP of $\sim$7 × 10^{-7} Torr. The ZnSe films were determined by high-resolution x-ray diffraction (HRXRD) to be single crystalline and well-oriented along the (001) direction. Although a small lattice mismatch of $\sim$1.0% is present between ZnSe and Zn_3P_2, the films were not coherently strained. Growth of CdS films by thermal evaporation occurred very slowly and required room temperature deposition and a higher BEP of $\sim$3 × 10^{-6} Torr. The CdS films were stoichiometric and polycrystalline, with a favored (0001) orientation.

Wurtzite ZnO films were grown in a separate vacuum chamber by RF sputter deposition using a sintered ZnO target. Various sputtering conditions were explored to minimize the electron carrier concentration in the ZnO. Higher doping levels were deleterious to the XPS measurement due to significant band bending near the heterojunction interface. The highest resistivity films were obtained for room temperature deposition using a 10% O$_2$/Ar gas mixture at 10 mTorr. The ZnO films were also polycrystalline with a strongly preferred (0001) orientation.

High-resolution XPS measurements on the bulk semiconductors and on heterostructure interfaces were performed in a Kratos surface-science instrument with a monochromatic Al Kα (1486.7 eV) x-ray source and a background pressure of <1 × 10^{-9} Torr. Excited photoelectrons were collected at 0° from the surface normal with a detection line width of <0.26 eV. All XPS measurements on the bulk semiconductor films were performed in duplicate. Reference measurements of the core-level and valence-band regions were collected on vacuum-cleaved (v.c.) single crystals of each bulk material, to minimize the contribution of surface contamination to the determination of the band offsets.

Interface measurements of $\Delta E_{CL,i}$ were collected for several thicknesses of each II-VI compound deposited onto a thick ($\sim$200 nm) Zn_3P_2 epilayer. The thickness of the II-VI film typically ranged from 0.2 nm to 3.0 nm. The group-V and group-VI core levels were chosen for the band offset measurements due to the high intensity and narrow peak widths of these signals. However, in the case of the ZnO/Zn_3P_2 interface, the O 1s core level was particularly sensitive

to even small amounts of contamination from adventitious H_2O and other surface hydroxide species. The Zn $3d$ core level was therefore used instead, and was found to be less surface sensitive while also showing contributions from both Zn–P and Zn–O bonding.

Peak fitting was used to accurately and reproducibly determine the core-level binding energies for all samples. Prior to fitting, photoelectron spectra were processed using a "Shirley" type baseline subtraction.[26] Core levels were modeled as doublets of weighted Gaussian-Lorentzian (G-L) product functions. The doublet peak area ratio and peak separation for a given core level were constrained across all samples. The peak area ratio was fixed to the theoretically expected relative intensities of excited electrons for a given symmetry (i.e., s, p, d, and f).[27] The doublet peak separation was constrained to the splitting value observed on the cleaved single crystals. The fitting parameters are summarized in Table II. The average position of the fitted doublet peaks was used as the absolute core-level binding energy for the subsequent offset calculations.

III. THEORETICAL METHODS

The VBM positions ($E_{VBM} - E_F$) of bulk Zn_3P_2 and of the II-VI materials of interest were determined by fitting the measured XPS valence-band region to a calculated valence-band density of states (VB-DOS). This technique is considered more accurate than simple linear extrapolation of the leading edge of the valence-band region.[28] In this process, the partial electronic DOS (PEDOS) for each material was calculated *ab initio* using hybrid density functional theory (DFT).

The DFT calculations were performed using the VASP[29,30] code, with the projector-augmented wave approach[31] used to describe the interaction between the core (Zn:[Ar], Cd:[Kr], S:[Ne], and O:[He]) and valence electrons. The calculations implemented the screened hybrid functional as proposed by Heyd, Scuseria, and Ernzerhof (HSE).[32] A percentage of the exact nonlocal Fock exchange (α) was added to the Perdew, Burke, and Ernzerhof[33] (PBE) functional with a screening of $\omega = 0.11$ bohr^{-1} applied in order to partition the Coulomb potential into long range (LR) and short range (SR) terms. The exchange and correlation terms are

$$E_{xc}^{HSE}(\omega) = E_x^{HSE,SR} + E_x^{PBE,LR} + E_C^{PBE}, \quad (3)$$

where

$$E_x^{HSE,SR} = \alpha E_x^{Fock,SR} + (1-\alpha)E_x^{PBE,SR}. \quad (4)$$

The Hartree-Fock and PBE exchanges are only mixed in the SR part, with the LR exchange interactions represented by the corresponding part of the range separated PBE functional.

To accurately reproduce the experimentally known band gaps and DOS features of Zn_3P_2, ZnO, CdS, and ZnSe, exchange values of 25%, 37.5%, 30%, and 32.5% were utilized, respectively. The HSE approach consistently produces structural and band gap data that are more accurate than standard density functional approaches, such as the local density approximation (LDA) or the generalized gradient approximation (GGA).[34–39] A cut-off value of 600 eV and a k-point mesh of $4 \times 4 \times 3$, $8 \times 8 \times 6$, $5 \times 5 \times 4$, and $6 \times 6 \times 6$, all centered on the Γ point, were found to be sufficient for Zn_3P_2, ZnO, CdS, and ZnSe, respectively.[40] All calculations were deemed to be converged when the forces on all atoms were less than 0.01 eV Å^{-1}.

The PEDOS contributions were weighted by the known x-ray photoionization cross section[41] of their respective atoms and were then summed, resulting in the total VB-DOS. The weighting was performed to accurately represent the processes that contributed to the experimental XPS data. The raw VB-DOS was then convoluted with an instrument-specific spectrometer response function and the results were then fit to the leading edge of the XPS data. The spectrometer response function was determined for the Kratos instrument by measurement of the Au $4f$ doublet. The Au spectrum was fit to a Voigt function assuming Gaussian broadening and an inherent Lorentzian linewidth of 0.317 eV. The details of the convolution and fitting procedure have been described previously.[28]

IV. RESULTS

A. Bulk semiconductor valence-band region

Figures 1(a)–1(d) display the x-ray photoelectron spectra of the valence-band region for the bulk Zn_3P_2 and II-VI compounds. Nearly identical spectra were obtained for thick films and vacuum-cleaved wafers (not shown), indicating negligible contribution from surface contamination. Along with the experimental data, Figs. 1(a)–1(d) also display the VB-DOS calculations after correction for the atomic scattering factors (Raw VB-DOS) as well as after convolution with the Kratos spectrometer response function (Conv. VB-DOS). Excellent qualitative agreement was observed between the structural features of the measurements and the

TABLE II. Core level fitting parameters and measured $E_{CL} - E_{VBM}$ values for the bulk Zn_3P_2 and II-VI semiconductors.

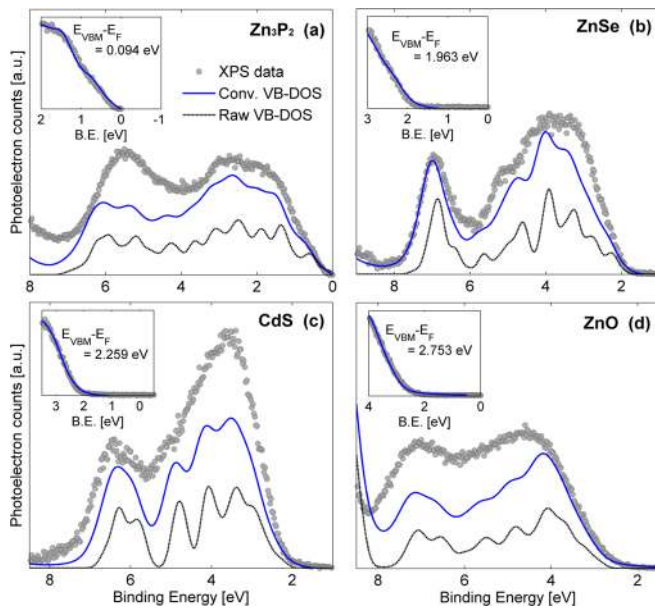| Material	Core level	Approx. B.E. (eV)	Peak fitting model	Doublet area ratio	Doublet separation (eV)	Measured $E_{CL} - E_{VBM}$ (eV)
Zn_3P_2	P $2p$	128.1	1:1 G-L	2:1	0.835	128.51 ± 0.02
	Zn $3d$	9.9	2:1 G-L	3:2	0.400	10.01 ± 0.02
ZnSe	Se $3d$	54.7	1:2 G-L	3:2	0.861	53.18 ± 0.04
CdS	S $2p$	162.2	1:2 G-L	1:1	1.200	160.45 ± 0.04
ZnO	Zn $3d$	9.9	Gaussian	3:2	0.810	7.60 ± 0.06

FIG. 1. High-resolution x-ray photoelectron spectra of the valence-band region measured on thick films of (a) Zn_3P_2, (b) ZnSe, (c) CdS, and (d) ZnO. For each material, the calculated VB-DOS are displayed before and after convolution with the spectrometer response function. The insets show the VBM position determined by fitting the convolved VB-DOS to the XPS data.

calculations. The inset of each figure displays the fit to the leading edge of the XPS data with the convolved VB-DOS, resulting in a value for the position of the VBM. The absolute value of the VBM differed from sample to sample due to small variations in doping. This behavior was especially true for vacuum-cleaved samples, which had intrinsic doping levels. Nevertheless, the relative position of the core-level binding energy to the VBM was very reproducible for each bulk material. Table II presents values of $E_{CL} - E_{VBM}$ measured for the bulk semiconductor compounds averaged over three samples, including the vacuum-cleaved wafers.

B. ZnSe/Zn₃P₂ band alignment

Figures 2(a) and 2(b) display the fitted XPS spectra of the P 2*p* and Se 3*d* core levels obtained from samples of varying ZnSe overlayer thickness grown on thick Zn_3P_2. The Zn_3P_2 P

2*p* core level was composed of two doublet pairs—an intense, low binding-energy doublet due to bulk Zn–P bonding, and a low-intensity, higher binding-energy doublet that has previously been attributed to surface/interfacial P–P bonding.[15,42] Upon heterojunction formation, little or no shift was observed in the bulk P 2*p* binding energy, but a ~0.7 eV shift toward lower binding energy was observed for the Se 3*d* core level. Only a small variation in $\Delta E_{CL,i}$ was observed with increasing ZnSe thickness, indicating minimal band bending in the overlayer. An average $\Delta E_{CL,i}$ of -74.12 ± 0.05 eV was calculated across five interface samples. Use of Eqs. (1) and (2) yielded ΔE_V of -1.21 ± 0.11 eV and ΔE_C of -0.03 ± 0.11 eV for the $ZnSe/Zn_3P_2$ heterojunction.

Figure 2(c) displays the energy-band diagram of an n-$ZnSe$/p-Zn_3P_2 heterojunction under equilibrium conditions, given the measured band discontinuities. The band bending across the interface was calculated using the AFORS-HET[43] device simulation package. The energy differences between the Fermi level and the conduction and valence bands ($\delta_n = E_C - E_F$, $\delta_p = E_F - E_V$) in the quasi-neutral region of each semiconductor were calculated assuming doping levels of $n = 1 \times 10^{18}$ cm^{-3} and $p = 1 \times 10^{17}$ cm^{-3} for ZnSe and Zn_3P_2, respectively. The offset measurement indicated an alignment of the ZnSe and Zn_3P_2 conduction bands within a few tenths of an eV, resulting in either a slightly type-I or type-II junction.

C. CdS/Zn₃P₂ band alignment

Figures 3(a) and 3(b) display the XPS data for the P 2*p* and S 2*p* core levels measured on thin CdS/Zn_3P_2 heterostructures having various CdS film thicknesses. Upon heterojunction formation, a ~0.3 eV shift towards lower binding energy was observed for the S 2*p* peaks, whereas a slight (~0.1 eV) shift toward higher binding energy was observed for the P 2*p* core level. The average value for $\Delta E_{CL,i}$ was 33.61 ± 0.04 eV, resulting in ΔE_V and ΔE_C values of -1.67 ± 0.10 eV and -0.76 ± 0.10 eV, respectively. The measured offsets yielded the calculated energy-band diagram of Fig. 3(c) for the n-CdS/p-Zn_3P_2 heterojunction. The CdS/Zn_3P_2 interface demonstrated a clear type-II alignment with a much larger conduction-band offset than was observed for the ZnSe/Zn_3P_2 interface.
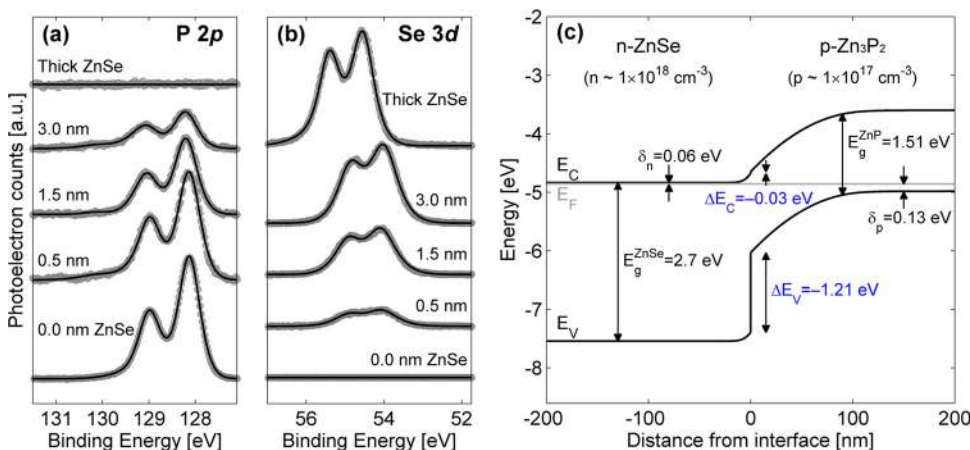

FIG. 2. Fitted XPS data of the (a) P 2*p* and (b) Se 3*d* core levels measured on ultrathin $ZnSe/Zn_3P_2$ heterojunction interfaces of increasing ZnSe overlayer thickness. (c) The energy-band alignment for an n$^+$-$ZnSe$/p-Zn_3P_2 heterojunction interface calculated given the measured ΔE_V and assumed doping levels of $n = 1 \times 10^{18}$ cm^{-3} and $p = 1 \times 10^{17}$ cm^{-3} for ZnSe and Zn_3P_2, respectively.
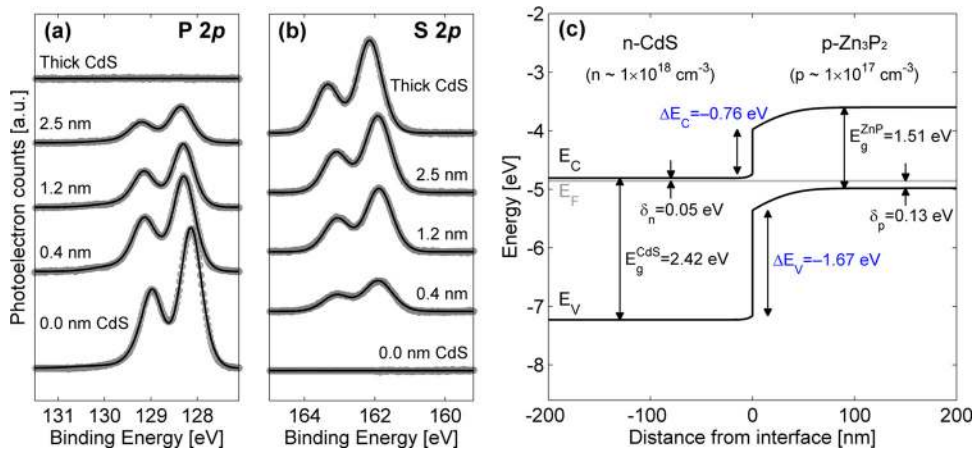
FIG. 3. Fitted XPS data of the (a) P 2*p* and (b) S 2*p* core levels measured on ultrathin CdS/Zn$_3$P$_2$ heterojunction interfaces of increasing CdS overlayer thickness. (c) The energy-band alignment for an n-CdS/p-Zn$_3$P$_2$ heterojunction interface calculated given the measured ΔE_V and assumed doping levels of n = 1 × 10^{18} cm^{-3} and p = 1 × 10^{17} cm^{-3} for CdS and Zn$_3$P$_2$, respectively.

D. ZnO/Zn$_3$P$_2$ band alignment

Figure 4(a) displays the Zn 3*d* core level spectra measured on ZnO/Zn$_3$P$_2$ heterostructures. Upon interface formation, two separate contributions were observed in the Zn 3*d* peak due to the presence of phosphide and oxide phases. These peaks were reproducibly discriminated by use of the fitting procedure described above. The binding energy of the phosphide peak remained constant as the thickness of the oxide layer increased. However, a shift of ~0.9 eV toward higher binding energy was observed for the interfacial oxide peak relative to the position of the bulk oxide peak. Additionally, a slow decrease in the separation of the core levels (equivalent to a decrease in the ΔE_V) was observed with increasing ZnO thickness, indicating that some band bending was present within the ZnO layer. The band bending resulted in a small decrease in the accuracy of the band-offset measurement. An average $\Delta E_{CL,i}$ of 1.10 ± 0.08 eV was measured across six interface samples, leading to calculated ΔE_V and ΔE_C values of −3.50 ± 0.16 eV and −1.61 ± 0.16, respectively, for this interface.

Figure 4(b) displays the energy-band diagram for an n-ZnO/p-Zn$_3$P$_2$ heterojunction. Based on the measured band discontinuities, the position of the ZnO conduction-band minimum (CBM) was located just below the Zn$_3$P$_2$ VBM, resulting in a slightly type-III or "staggered" alignment. The ZnO conduction and valence bands were bent sharply downward in energy at the interface, due to the abnormal staggered band alignment with Zn$_3$P$_2$. This behavior is in the opposite direction of the type-II alignment that was observed in the band diagrams for ZnSe/Zn$_3$P$_2$ and CdS/Zn$_3$P$_2$. The calculated band bending qualitatively agreed with the trend in the XPS core-level separation that was observed for increasing oxide thickness.

V. DISCUSSION

A. II-VI/Zn$_3$P$_2$ band offsets—Measurement versus prediction

Figure 5 compares the measured band alignments for the II-VI/Zn$_3$P$_2$ heterojunctions with the values predicted by various approaches including the Anderson electron affinity (EA) model,[16] an interface dipole model,[44] and available DFT calculations.[45] The plotted Zn$_3$P$_2$ CBM was fixed at −3.6 eV with respect to the vacuum level, based on a reported value of the Zn$_3$P$_2$ electron affinity (χ).[46] The ZnS/Zn$_3$P$_2$ band alignment has been reported previously and was
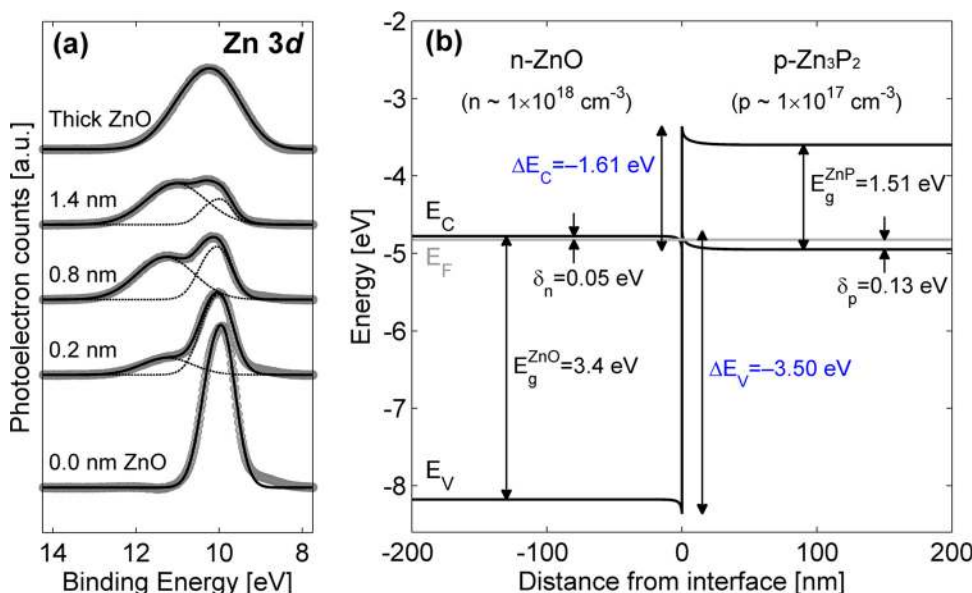

FIG. 4. (a) Fitted XPS data of the Zn 3*d* core level for sputter-deposited ZnO/Zn$_3$P$_2$ heterojunction interfaces with increasing ZnO thickness. The interface peaks show contributions from both the phosphide and oxide states. (b) The energy-band alignment for an n-ZnO/p-Zn$_3$P$_2$ heterojunction interface calculated given the measured ΔE_V and assumed doping levels of n = 1 × 10^{18} cm^{-3} and p = 1 × 10^{17} cm^{-3} for ZnO and Zn$_3$P$_2$, respectively.
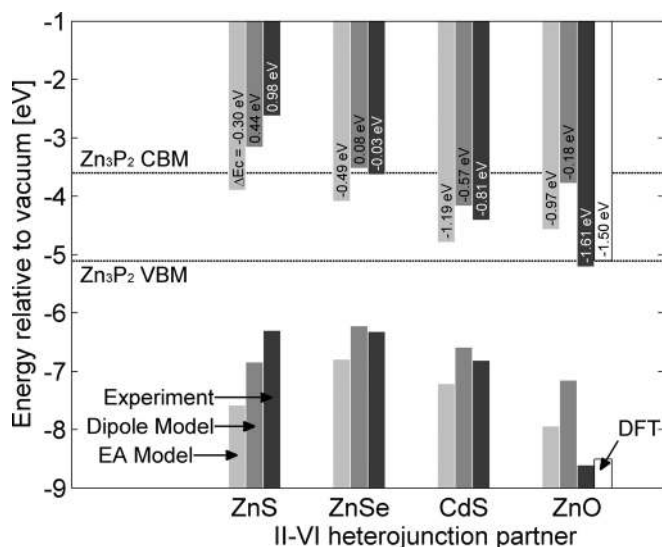
FIG. 5. A comparison of experimentally measured II-VI/Zn_3P_2 heterojunction band offsets with those predicted from the EA model,[16] an effective interface dipole model,[44] and universal hydrogen-level alignment calculations.[45] The ZnS/Zn_3P_2 band offset measurement has been reported previously.[15] The CBM of Zn_3P_2 was fixed at -3.6 eV with respect to the vacuum level based on the reported electron affinity.[46]

obtained using similar techniques to those used herein.[15] Table I presents the χ values for each II-VI material used in the EA and dipole-model calculations. Figure 5 clearly indicates the presence of a large (≥ 0.4 eV) discrepancy between the EA model and the measured ΔE_C, indicating the presence of more complicated bulk and/or surface phenomena.

The dipole model proposed by Ruan and Ching[44] is a first-order correction to the EA model, and in general results in improved predictions of ΔE_C, especially for ZnS, ZnSe, and CdS heterojunctions. Assuming defect-free interfaces, the model calculates the effective interfacial dipole resulting from charge transfer from the higher valence-band material (Zn_3P_2) to the lower valence-band material (II-VI) and thus predicts the extent to which the band offsets are modified. The dipole model gives the best prediction for the ZnSe/Zn_3P_2 heterojunction, which has the smallest lattice mismatch of all the systems and therefore is likely to have the lowest density of interfacial defects. The interface dipole model is also very sensitive to the value of the hole effective masses of Zn_3P_2, which are poorly known. In this work, the Zn_3P_2 hole effective masses were approximated by fitting a parabolic function to the valence-band structure of Zn_3P_2 that was calculated by DFT. The values of these fits are presented in Table III for each of the principal axis directions. The discrepancy between the prediction of the dipole model

TABLE III. Calculated effective mass values (m_h/m_o) for the three uppermost valence bands of Zn_3P_2 as determined by parabolic fitting of the Zn_3P_2 band diagram. ν_1 corresponds to the highest energy, or "heavy hole," valence band.

Principle axis	ν_1	ν_2	ν_3
$\Gamma \to Z$	0.255	0.760	0.761
$\Gamma \to X$	0.407	3.770	0.109
$\Gamma \to M$	0.415	0.410	0.141

and the measured offsets is consistent with a possible inaccuracy in the effective masses or with a modification in the values of the effective masses upon interface formation.

Both the EA model and the effective interface dipole model failed to even qualitatively predict the ZnO/Zn_3P_2 band offsets. However, the ΔE_V of -3.4 eV calculated by Limpijumnong and coworkers using DFT is in excellent agreement with the value of -3.5 eV measured herein. The calculation assumed universal alignment of the electronic transition levels of H interstitials in the two semiconductors.[47] The agreement between the theory and experiment suggests that the staggered band alignment observed for ZnO/Zn_3P_2 is not a result of an interface dipole or surface reconstruction, but is inherent to the bulk materials system.

B. Band alignment and photovoltaic device performance

The measured band discontinuities of the II-VI/Zn_3P_2 interfaces are well correlated with the previously reported device performance for these heterojunctions. For instance, the alignment of the ZnSe and Zn_3P_2 conduction bands suggests that a large barrier height should be attainable for a ZnSe/Zn_3P_2 solar cell. Bhushan *et al.* demonstrated V_{OC}'s as high as 810 mV and diffusion voltages (V_D) >1.4 V for superstrate Zn_3P_2/ZnSe solar cells.[14] Under ideal conditions (i.e., removal of all non-radiative recombination pathways), the barrier height of these ZnSe/Zn_3P_2 heterojunctions approached the value of the band gap of Zn_3P_2. The ZnSe/Zn_3P_2 conduction-band alignment also implies facile electron transport across the junction as well as a hole-blocking layer due to the large valence-band offset. Combined, these characteristics result in good carrier separation at the heterojunction interface, consistent with the relatively high reported V_{OC}'s for this system. The superstrate design ultimately limited the overall device performance because the solar cell was illuminated on the back side of the Zn_3P_2, resulting in a large amount of carrier recombination at the back contact and therefore low J_{SC}'s. Thus, improved performance should be attainable with a substrate device in which the ZnSe is deposited directly onto the Zn_3P_2 surface.

Conversely, the measured $\Delta E_C = -0.76$ eV for the CdS/Zn_3P_2 interface results in a maximum possible barrier height of ~ 700 mV. This value is in good agreement with the V_D of 640 mV for CdS/Zn_3P_2 that had been reported by Suda and coworkers.[13] The low attainable barrier height of the CdS/Zn_3P_2 heterojunction will therefore limit the maximum efficiency of these types of solar cells. One possible way to manipulate the conduction-band offset between CdS and Zn_3P_2 is to use a $Cd_xZn_{1-x}S$ emitter. The ZnS/Zn_3P_2 heterojunction has been reported to have a conduction-band spike of ~ 1 eV, therefore, a $Cd_xZn_{1-x}S$ alloy should facilitate tuning of the position of the conduction band to closely match that of Zn_3P_2, in accord with reports in the literature.[14] Alloying would also increase the band gap of the emitter over that of CdS and in principle create a better lattice match with Zn_3P_2 as compared to either CdS or ZnS alone, resulting in better collection efficiency at shorter wavelengths of light and a lower density of interfacial defects.

Based on the measured energy-band alignment, the conduction band of ZnO forms a tunnel junction with the Zn_3P_2 valence band. This prediction is not in accord with the observation that ZnO/Zn_3P_2 heterojunction photovoltaic devices reported by Nayar *et al.* showed V_{OC}'s as high as 300 mV. Their devices were fabricated on freshly etched Zn_3P_2 ($p \sim 2 \times 10^{15}\,cm^{-3}$) followed by several minutes of sputter cleaning, with the ZnO films deposited by co-sputtering of ZnO and Zn metal using pure Ar. Possible mechanisms for creation of a barrier include:

(1) Formation of a $Zn_x(PO_3)y$ interfacial layer during sputter deposition. A layer of ill-defined oxide composition could produce a significantly altered band alignment with Zn_3P_2 and thus a measurable barrier height in a photovoltaic device.
(2) Formation of a rectifying Schottky contact with metal precipitates at the ZnO/Zn_3P_2 interface.
(3) Formation of an n-type inversion layer at the surface of the Zn_3P_2 resulting in a buried homojunction.

Mechanism (1) is not likely to be the cause of the barrier height in the ZnO/Zn_3P_2 heterojunction because little to no oxidation was observed for the Zn_3P_2 P 2*p* core level after ZnO deposition under a 10% O_2 partial pressure used herein. A $Zn_x(PO_3)_y$ layer of significant thickness is therefore unlikely to have formed under the less-oxidizing sputtering conditions used by Nayar and Catalano. Furthermore, Zn metal has been reported to form an ohmic contact with Zn_3P_2,[48] eliminating the prospect of mechanism (2), Schottky barrier formation at this interface. Mechanism (3) therefore represents a more likely explanation for the observed barrier height. The formation of an inversion layer at the Zn_3P_2 surface is not apparent from the band diagram of the ZnO/Zn_3P_2 heterostructure. The tunnel junction formation instead favors hole accumulation at the Zn_3P_2 surface, which has been proposed as an alternative mechanism for the p-type conductivity in P-doped ZnO films.[45] However, fixed positive charge at the ZnO/Zn_3P_2 interface could induce an inversion layer in weakly p-type Zn_3P_2, in accord with suggestions of such behavior at oxidized Zn_3P_2 surfaces.[49]

VI. CONCLUSION

The energy-band alignments have been established for heterojunctions of ZnSe, CdS, and ZnO n-type semiconductors grown on Zn_3P_2. The $ZnSe/Zn_3P_2$ interface had a negligible conduction-band offset and a large hole-blocking barrier, demonstrating an optimal alignment for a heterojunction solar cell. This ideal alignment is reflected in the significant open-circuit photovoltages and large barrier heights reported for $ZnSe/Zn_3P_2$ solar cells. The CdS/Zn_3P_2 heterojunction was type-II, with a much larger conduction-band offset than for $ZnSe/Zn_3P_2$. This behavior accounts for the inferior V_{OC} observed for CdS/Zn_3P_2 heterojunctions relative to $ZnSe/Zn_3P_2$ heterojunctions. However, the offset can potentially be modified by the use of $Cd_xZn_{1-x}S$ ternary alloys, which should result in a more ideal band alignment and a larger emitter band gap. The ZnO/Zn_3P_2 interface was found to have an unusual type-III alignment that resulted in a

tunnel junction between the ZnO and Zn_3P_2. The offset was poorly predicted by electron affinity and interface dipole models, but was well described by universal H-level alignment theory, which suggests the band alignment is intrinsic to the bulk semiconductors. The barrier heights reported for ZnO/Zn_3P_2 heterojunction solar cells therefore likely arise from mixed composition or surface states at the interface.

[1]G. M. Kimball, A. M. Müller, N. S. Lewis, and H. A. Atwater, Appl. Phys. Lett. **95**, 112103 (2009).
[2]J. M. Pawlikowski, Phys. Rev. B **26**, 4711 (1982).
[3]G. M. Kimball, N. S. Lewis, and H. A. Atwater, paper presented at 35th IEEE Photovoltaic Specialists Conference (PVSC) (2010).
[4]M. Bhushan and A. Catalano, Appl. Phys. Lett. **38**, 39 (1981).
[5]R. C. Schoonmaker, A. R. Venkitaraman, and P. K. Lee, J. Phys. Chem. **71**, 2676 (1967).
[6]C. Wadia, A. P. Alivisatos, and D. M. Kammen, Environ. Sci. Technol. **43**, 2072 (2009).
[7]S. B. Demers and A. Van de Walle, Phys. Rev. B **85**, 195208 (2012).
[8]W. Yin and Y. Yan, J. Appl. Phys. **113**, 013708 (2013).
[9]M. Bhushan, Appl. Phys. Lett. **40**, 51 (1982).
[10]M. S. Casey, A. L. Fahrenbruch, and R. H. Bube, J. Appl. Phys. **61**, 2941 (1987).
[11]T. Suda, M. Suzuki, and S. Kurita, Jpn. J. Appl. Phys., Part 2 **22**, L656 (1983).
[12]P. S. Nayar and A. Catalano, Appl. Phys. Lett. **39**, 105 (1981).
[13]T. Suda, A. Kuroyanagi, and S. Kurita, in *Technical Digest, International PVSEC-1, Kobe, Japan* (1984), p. 381.
[14]M. Bhushan and J. D. Meakin, *Zn₃P₂ as an Improved Semiconductor for Photovoltaic Solar Cells: Final Report, April 1983–March 1984*. (University of Delaware, Institute of Energy Conversion; Solar Energy Research Institute, Golden, CO, 1985).
[15]J. P. Bosco, S. B. Demers, G. M. Kimball, N. S. Lewis, and H. A. Atwater, J. Appl. Phys. **112**, 093703 (2012).
[16]R. L. Anderson, Solid-State Electron. **5**, 341 (1962).
[17]A. Franciosi and C. G. Van de Walle, Surf. Sci. Rep. **25**, 1 (1996).
[18]E. A. Kraut, R. W. Grant, J. R. Waldrop, and S. P. Kowalczyk, Phys. Rev. Lett. **44**, 1620 (1980).
[19]J. P. Bosco, G. M. Kimball, N. S. Lewis, and H. A. Atwater, J. Cryst. Growth **363**, 205 (2013).
[20]A. Catalano, J. Cryst. Growth **49**, 681 (1980).
[21]S. Fuke, Y. Takatsuka, K. Kuwahara, and T. Imai, J. Cryst. Growth **87**, 567 (1988).
[22]K. Ohkawa, S. Yoshii, H. Takeishi, A. Tsujimura, S. Hayashi, T. Karasawa, and T. Mitsuyu, Jpn. J. Appl. Phys., Part 2 **33**, L1673 (1994).
[23]R. M. Park, H. A. Mar, and N. M. Salansky, J. Vac. Sci. Technol. B **3**, 676 (1985).
[24]J. Lee, Appl. Surf. Sci. **252**, 1398 (2005).
[25]M. G. Faraj and K. Ibrahim, J. Mater. Sci.: Mater. Electron. **23**, 1219 (2012).

[26]D. A. Shirley, Phys. Rev. B **5**, 4709 (1972).

[27]D. Briggs and P. Seah, *Practical Surface Analysis: Auger and X-Ray Photoelectron Spectroscopy* (Wiley, 1990).

[28]E. A. Kraut, R. W. Grant, J. R. Waldrop, and S. P. Kowalczyk, Phys. Rev. B **28**, 1965 (1983).

[29]G. Kresse and J. Furthmüller, Comput. Mater. Sci. **6**, 15 (1996).

[30]G. Kresse and J. Hafner, Phys. Rev. B **49**, 14251 (1994).

[31]P. E. Blöchl, Phys. Rev. B **50**, 17953 (1994).

[32]A. V. Krukau, O. A. Vydrov, A. F. Izmaylov, and G. E. Scuseria, J. Chem. Phys. **125**, 5 (2006).

[33]J. P. Perdew, K. Burke, and M. Ernzerhof, Phys. Rev. Lett. **77**, 3865 (1996).

[34]J. P. Allen, D. O. Scanlon, and G. W. Watson, Phys. Rev. B **81**, 161103 (2010).

[35]M. Burbano, D. O. Scanlon, and G. W. Watson, J. Am. Chem. Soc. **133**, 15065 (2011).

[36]A. B. Kehoe, D. O. Scanlon, and G. W. Watson, Phys. Rev. B **83**, 035410 (2011).

[37]D. O. Scanlon, A. Walsh, and G. W. Watson, Chem. Mater. **21**, 4568 (2009).

[38]D. O. Scanlon and G. W. Watson, J. Phys. Chem. Lett. **1**, 3195 (2010).

[39]D. O. Scanlon and G. W. Watson, Phys. Chem. Chem. Phys. **13**, 9667 (2011).

[40]See supplementary material at http://dx.doi.org/10.1063/1.4807646 for the DFT energy band diagram and PEDOS of each bulk semiconductor material as well as for a full list of the experimentally determined XPS core level peak positions for all of the samples studied in this work.

[41]J. J. Yeh and I. Lindau, At. Data Nucl. Data Tables **32**, 1 (1985).

[42]G. M. Kimball, J. P. Bosco, A. M. Muller, S. F. Tajdar, B. S. Brunschwig, H. A. Atwater, and N. S. Lewis, J. Appl. Phys. **112**, 106101 (2012).

[43]R. Stangl, M. Kriegel, S. Kirste, M. Schmidt, and W. Fuhs, in Proceedings of IEEE Photovoltaics Specialists Conference Orlando, FL, USA (2005).

[44]Y. C. Ruan and W. Y. Ching, J. Appl. Phys. **62**, 2885 (1987).

[45]S. Limpijumnong, L. Gordon, M. Miao, A. Janotti, and C. G. Van de Walle, Appl. Phys. Lett. **97**, 072112 (2010).

[46]A. J. Nelson, L. L. Kazmerski, M. Engelhardt, and H. Hochst, J. Appl. Phys. **67**, 1393 (1990).

[47]C. G. Van de Walle and J. Neugebauer, Nature **423**, 626 (2003).

[48]N. C. Wyeth and A. Catalano, J. Appl. Phys. **51**, 2286 (1980).

[49]S. Hava, J. Appl. Phys. **59**, 4097 (1986).

[50]C. Koughia, S. Kasap, and P. Capper, *Springer Handbook of Electronic and Photonic Materials* (Springer, 2007).

[51]C. Kittel, *Introduction to Solid State Physics* (John Wiley & Sons, 2004).

[52]W. M. Haynes, D. R. Lide, and T. J. Bruno, *CRC Handbook of Chemistry and Physics* (CRC Press, 2012).

[53]R. K. Swank, Phys. Rev. **153**, 844 (1967).